Nuclear Instruments and Methods in Physics Research A 1064 (2024) 169437

Contents lists available at ScienceDirect

Nuclear Inst. and Methods in Physics Research, A

journal homepage: www.elsevier.com/locate/nima

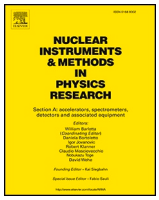

Full Length Article

# A quasi-spherical optical module QSM-6M based on the Hamamatsu R877 PMT for the detection of Cherenkov radiation in water

M.B. Amelchakov [a], A.G. Bogdanov [a], A. Chiavassa [b,c,*], D.M. Gromushkin [a], A.N. Dmitryeva [a], T.A. Karetnikova [a], S.S. Khokhlov [a,**], V.V. Kindin [a], R.P. Kokoulin [a], K.G. Kompaniets [a], A. Yu Konovalova [a], G. Mannocchi [d], N.A. Pasyuk [a], A.A. Petrukhin [a], I.A. Shulzhenko [a], V.V. Shutenko [a], G. Trinchero [c,d], I.I. Yashin [a]

[a] National Research Nuclear University MEPhI (Moscow Engineering Physics Institute), 115409, Moscow, Russia
[b] Dipartimento di Fisica Dell' Università Degli Studi di Torino, 10125, Torino, Italy
[c] Sezione di Torino Dell' Istituto Nazionale di Fisica Nucleare – INFN, 10125, Torino, Italy
[d] Osservatorio Astrofisico di Torino – INAF, 10025, Torino, Italy

ARTICLE INFO

*Keywords:*
Optical module
Quasi-spherical module
Hamamatsu R877 PMT
Cherenkov neutrino telescopes
Cherenkov water calorimeter NEVOD

ABSTRACT

In this paper, we describe the quasi-spherical optical module QSM-6M to detect Cherenkov radiation in water. The module is based on six photomultiplier tubes (PMTs) with flat photocathodes Hamamatsu R877. We discuss the results of the photomultiplier testing, as well as the choice of the high-voltage divider providing the PMT dynamic range from 1 to $10^5$ photoelectrons. The techniques for studying QSM-6M characteristics, as well as the results of the underwater testing of the module for an 18-month period are presented. We also present the results of the analysis of the QSM-6M response to single-muon and multiparticle events detected by the installations of the Experimental Complex NEVOD.

## 1. Introduction

Cherenkov radiation, discovered in 1943 [1], became widespread in the second half of the 20th century, when detectors with a mass of several kilotons were required to search for proton decay and studying exotic processes. To solve these problems, Cherenkov water detectors with a peripheral detecting system, in which the volume of the detector is viewed by an array of photomultipliers mounted on the walls of the detector, were constructed. These detectors can measure particles from any direction, i.e. they are 4π detectors. Examples of such detectors are IMB [2], Kamiokande [3], SNO [4], etc.

To study high-energy neutrinos, detectors with a mass of tens and hundreds of megatons were required. Large-volume installations cannot be constructed based on a peripheral detecting system, since photons of Cherenkov radiation produced in events occurring in the center of the detector do not reach photomultipliers due to the attenuation of light in water. To date, the largest installation with a peripheral detecting system is the Super Kamiokande detector with a mass of 50 kilotons [5].

To achieve large volumes, the development of detectors with a spatial lattice of vertical garlands of optical modules began in the second half of the 1970s. The first example was the DUMAND detector [6,7]. Since the efficiency of recording physical events and the accuracy of reconstructing their parameters depend on the optical module design, the corresponding requirements for optical modules were formulated [8]. One of these requirements is the largest possible angle of Cherenkov radiation reception.

In 1979 at the 16th International Cosmic Ray Conference, the idea of a quasi-spherical module (QSM) detecting Cherenkov radiation at a solid angle of 4π was proposed [9]. According to the proposed concept, a quasi-spherical module can be formed by photomultipliers with flat photocathodes located in the vertices, centers of faces or edges of regular polyhedra. Four of the five regular polyhedra, except a tetrahedron, can be used to create a quasi-spherical module: hexahedron, octahedron, dodecahedron and icosahedron [10]. When recording a wave with a flat front, the sum of the squared response amplitudes of photomultipliers for such QSM configurations does not depend on the arrival direction.

A quasi-spherical module of a simplest design, QSM-6, consists of six photomultipliers directed along the axes of the orthogonal coordinate

* Corresponding author. Dipartimento di Fisica Dell' Università Degli Studi di Torino, 10125, Torino, Italy.
** Corresponding author.
*E-mail addresses:* andrea.chiavassa@unito.it (A. Chiavassa), SSKhokhlov@mephi.ru (S.S. Khokhlov).

https://doi.org/10.1016/j.nima.2024.169437
Received 30 January 2024; Received in revised form 9 May 2024; Accepted 9 May 2024
Available online 17 May 2024

system (Fig. 1).

If the PMT response is proportional to the cosine of the angle of Cherenkov radiation arrival at the photocathode $A_{x,\,y,\,z} = A\cos\alpha_{x,\,y,\,z}$, then the QSM-6 response does not depend on the arrival direction:

$$B = \sqrt{{A_x}^2 + {A_y}^2 + {A_z}^2} = \sqrt{A^2\left(\cos^2\alpha_x + \cos^2\alpha_y + \cos^2\alpha_z\right)} = A \qquad (1)$$

In 1994, the first version of the Cherenkov water detector NEVOD was realized with the quasi-spherical modules QSM-6 [11]. These optical modules were equipped with FEU-49B photomultipliers with a multi-alkaline flat photocathode with a diameter of 15 cm.

Since we know the signals from individual photomultipliers and the total response, it is possible to determine the directional cosines and, correspondingly, the arrival direction of the Cherenkov radiation. A lattice of such modules allows determining particle trajectory and direction without using the time-of-flight method. This property of quasi-spherical modules allowed to detect, for the first time, the neutrino events on the Earth's surface using the spatial lattice of the NEVOD detector [12].

For a long time, the idea of using quasi-spherical modules when constructing large-scale Cherenkov water detectors was underestimated. Optical modules were developed based on hemispherical photomultipliers installed inside glass spherical housings. It was planned to use such modules in the DUMAND project. The first version of the module was equipped with the 15-inch hybrid photomultiplier Philips XP2600 with an electron-optical preamplifier [8]. The second version was developed based on a large-sized hemispherical photomultiplier Hamamatsu R2018 with a 15-inch photocathode [13].

The DUMAND project was not completed, but its ideas greatly influenced the designs of other detectors, whose modules were developed based on a single photomultiplier. The optical modules of the Baikal neutrino telescope NT-200 contained one QUASAR-370 photomultiplier with a diameter of 37 cm [14]. The modules were connected in pairs, and their coincidence was used to suppress PMT noise. However, the photocathodes were directed downwards, which limited the angle of Cherenkov radiation reception of a pair of modules. The Baikal-GVD detector is a development of the NT-200 neutrino telescope. Its optical modules contain one 10-inch Hamamatsu R7081-100 photomultiplier [15]. The optical modules of the AMANDA sub-ice detector

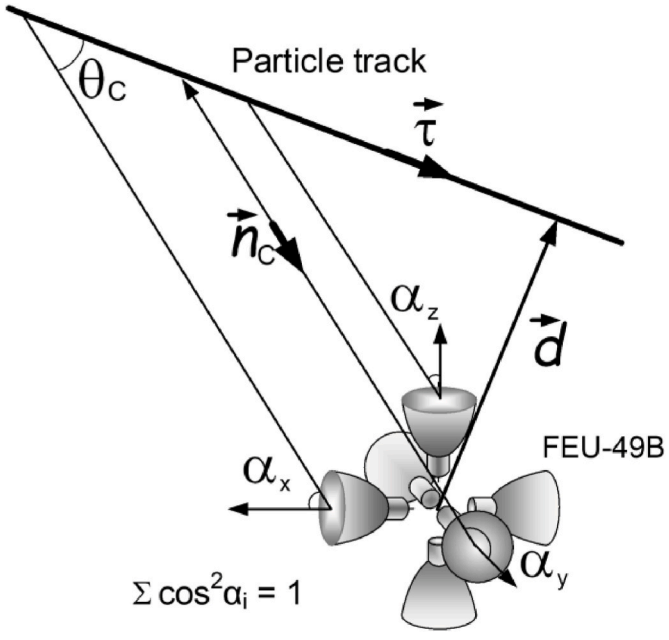


**Fig. 1.** Diagram of Cherenkov radiation detection with the quasi-spherical module QSM-6.

contained one 8-inch Hamamatsu R5912-2 photomultiplier [16]. An evolution of the AMANDA detector is the largest neutrino telescope IceCube. The IceCube optical modules include one 10-inch hemispherical Hamamatsu R7081-02 PMT [17]. The optical modules of the ANTARES detector also contain one 10-inch Hamamatsu R7081-20 photomultiplier [18,19]. The modules are combined in groups of three into storeys, and each module of a storey is inclined at 45° below the horizon. Such a system resembles a quasi-spherical module, but it is not sensitive to direct Cherenkov radiation from the upper hemisphere.

The idea of quasi-spherical modules has gained acceptance in the development of optical modules for neutrino telescopes of new generation. For the KM3NeT neutrino telescope [20], which is an evolution of the ANTARES detector, an optical module with a diameter of 17″ was developed [21]. It consists of 31 photomultipliers with a photocathode diameter of 3". The KM3NeT module does not contain an upward-directed photomultiplier tube, but due to the large number of PMTs, the module is sensitive to light at a solid angle of 4π, so it can be considered quasi-spherical.

The IceCube-Upgrade is a new part of the IceCube Observatory which is being constructed to improve the detectors' performance during observation of low-energy neutrinos, as well as for calibrations purposes. For this project, two new optical module designs have been proposed. The first one, mDOM (multi-PMT Digital Optical Module), is similar to the KM3NeT module. But the mDOM, having approximately the same size (410 mm), contains 24 photomultipliers with a diameter of 3" [22]. The second design is called D-Egg (Dual optical sensors in an Ellipsoid Glass for Gen2) [23]. It has the shape of an ellipsoid containing two Hamamatsu R5912-100-70 photomultipliers with a diameter of 8". One PMT is directed to the lower hemisphere, the second one – to the upper hemisphere. It is worth noting that, although the D-Egg is capable of detecting Cherenkov radiation in a solid angle of 4π, it cannot be classified as quasi-spherical, since its response depends on the radiation arrival direction.

The first version of the quasi-spherical modules QSM-6 based on FEU-49B photomultiplier had a small dynamic range, which did not allow the Cherenkov water detector NEVOD to operate in a calorimetric mode. In 2008–2010, the measuring system of the Cherenkov water detector NEVOD was upgraded. The second version of quasi-spherical modules was realized with the FEU-200 photomultiplier with a bi-alkaline photocathode. That ensured the dark current reduction by an order of magnitude. The readout of signals from the 12th and 9th dynodes of each photomultiplier made it possible to achieve a total dynamic range from 1 to $10^5$ photoelectrons (ph. e.) [24]. This wide dynamic range allowed the Cherenkov water detector NEVOD to operate in calorimetric mode, measuring Cherenkov radiation from cascades generated by single muons [25] and the energy deposit of muon bundles [26].

For the further development of the Experimental Complex NEVOD [27], conducting multicomponent studies of cosmic rays and studying the "muon puzzle" [28–30], we are constructing the detector TREK completely covering the side aperture of the Cherenkov water detector [31]. For more efficient joint operation of the Cherenkov water calorimeter (CWC) and the TREK detector, it is planned to upgrade the recording system of the CWC, to increase the effective volume of the spatial lattice from 800 to 1200 $m^3$ and to make it symmetrical with respect to the TREK detector.

To expand the spatial lattice, we require a new quasi-spherical module with good calorimetric characteristics and high efficiency in reconstructing single muon tracks. The FEU-200 photomultiplier used in QSM-6 has a louvered dynode system, which reduces the energy resolution of the module and makes it difficult to adjust the PMT gain due to a poorly defined single-electron peak. The new quasi-spherical module QSM-6M was developed based on the Hamamatsu R877 photomultiplier. This type of PMT has never before been used to detect Cherenkov radiation in water.

## 2. Characteristics of the hamamatsu R877 PMT

The Hamamatsu R877 photomultiplier has a 10-stage box dynode system and a bi-alkaline flat photocathode with a sensitive zone diameter of at least 111 mm. The maximum spectral sensitivity is achieved at the light wavelength of 420 nm. The quantum efficiency for this wavelength is 25% [32], which is noticeably higher than the quantum efficiency of the FEU-200 (15%). The outer diameter of the Hamamatsu R877 PMT bulb is 133 mm. This is slightly smaller than the outer diameter of the FEU-200 bulb (170 mm), which allows using the same module housing. We have studied the spectrometric and time characteristics of six Hamamatsu R877 photomultipliers. Since the parameters of tested photomultipliers have close values, in this section, when discussing a specific characteristic, we present only one typical dependence.

### 2.1. High-voltage divider and linearity range

To ensure the calorimetric mode, the dynamic range of the photomultiplier from 1 to $10^5$ ph. e. is required. In QSM-6, such a range was achieved by dual-dynode signal readout from the FEU-200. The linearity range of signals from the 12th dynode ($D_{12}$) is 1–1000 ph. e., and the range of the 9th dynode ($D_9$) is $10^2$–$10^5$ ph. e. The range from 100 to 1000 ph. e. is used to determine the cross-linking coefficients. To obtain a large dynamic range with the Hamamatsu R877 photomultiplier, we also use dual-dynode signal readout.

The characteristics of the Hamamatsu R877 PMT were studied using a measurement setup, which includes a box with a Teflon diffuser [33], installed on the box bottom and covering two KingBright L-7113NBC light-emitting diodes (LEDs) with a wavelength of 445 nm and a spectral line width at half maximum of 40 nm [34]. The duration of the LED flash is 6 ns [35]. The distance between the center of the tested PMT photocathode and the diffuser is 150 mm. LED is flashed by a dedicated illumination controller. The controller is synchronized with the CAEN V1729 unit, digitizing PMT signals with a sampling rate of 2 Gsps.

The study of the linearity range of the Hamamatsu R877 photomultiplier was carried out by the paired illumination method. It is assumed, that photomultiplier operates in the linear region if its response to illumination by two LEDs simultaneously is approximately equal to the sum of the responses to illumination by each LED separately. For numerical assessment, the non-linearity coefficient is used. It is calculated by the following formula:

$$\alpha = \frac{Q_{1+2} - (Q_1 + Q_2)}{Q_1 + Q_2} \bullet 100\%, \quad (2)$$

where $Q_{1+2}$ is the average value of the response charge when the photocathode is illuminated by simultaneous flashes from two LEDs; $Q_1$ and $Q_2$ are the average charges of the responses to illumination by the first and second LEDs separately. Average responses were calculated from response spectra for 500 LED flashes. It is assumed that the photomultiplier operates in a linear mode, if the absolute value of non-linearity coefficient is less than 5%.

The linearity range was measured using various circuits of supply voltage divider. Initially, we used two circuits recommended by the PMT manufacturer. In the first circuit ("standard" divider) shown in Fig. 2, all resistors between the dynodes are the same $R_i = 820$ kΩ, that ensures the same potential difference between the dynodes. The ballast resistor $R_{15}$ is used for adjustment. In the second circuit ("tapered" divider) several resistor values from Fig. 2 were replaced: $R_{10} = 1.2$ MΩ, $R_{11} = 2.0$ MΩ, $R_{12} = 2.5$ MΩ and $R_{14} = 1.8$ MΩ. This provides increasing potential differences between the senior dynodes starting from the 7th one. The linearity studies were performed for signals from the 10th and 7th dynodes.

With a "standard" divider and a dynode system gain of $M = 10^6$, the signals from the 10th dynode become non-linear at magnitudes of more than 750 pC. This corresponds to the linearity range $D_{10} = 1$–4700 ph. e. However, the signals from the 7th dynode become non-linear at a charge of only 65 pC. At the same time, the inter-dynode gain is $m_{10/7} = 150$. Thus, reading out signals from the 10th and 7th dynodes with a "standard" divider provides the dynamic range $D = 1$–$6 \times 10^4$ ph. e.

With a "tapered" divider, the upper value of the 10th dynode linearity range at the dynode system gain of $M = 10^6$ is 2600 pC, and 50 pC for the 7th dynode, the inter-dynode gain is $m_{10/7} = 200$. Thus, dual-dynode readout of signals with a "tapered" divider provides the dynamic range $D = 1$–$6.2 \times 10^4$ ph. e. which is close to that with a "standard" divider.

An increase in the dynamic range of signals from the 7th dynode was achieved with an optimized voltage divider in which the potential difference between 5th, 6th and 7th dynodes increases progressively. The circuit of the optimized divider is shown in Fig. 3.

Fig. 4 shows the non-linearity coefficients as functions of signal charge when using the optimized divider. Signals from the 10th and 7th dynodes are linear up to charge of 600 pC and 160 pC, correspondingly. The charge of the minimum distinguishable signal is ~0.15 pC. At a dynode system gain of $M = 10^6$ the inter-dynode gain is $m_{10/7} = 100$. Thus, the use of the optimized divider allows us to obtain dynamic ranges $D_{10} = 1$–3750 ph. e. for the 10th dynode and $D_7 = 10^2$–$10^5$ ph. e. for the 7th dynode.

### 2.2. Dynode system gain

For the Hamamatsu R877 photomultiplier with a modified divider, we have measured the dependence of the dynode system gain on the supply voltage. To do this, it is necessary to reliably measure the gain of the PMT dynode system at some supply voltage (can be arbitrarily chosen), i.e. to get a reference point.

The dynode system gain was measured using the method of single-electron illumination. The probability $P$ of knocking out $n$ photoelectrons from the photocathode is described by the Poisson distribution:

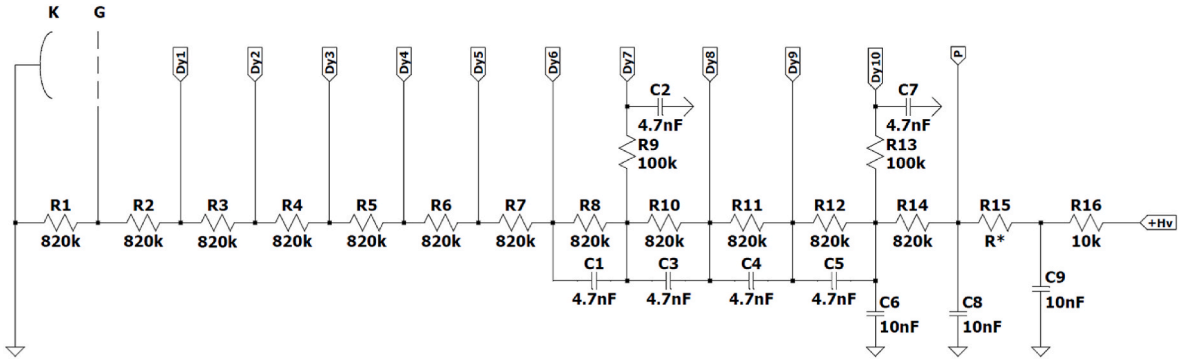


**Fig. 2.** The circuit of the "standard" voltage divider for the Hamamatsu R877 PMT.

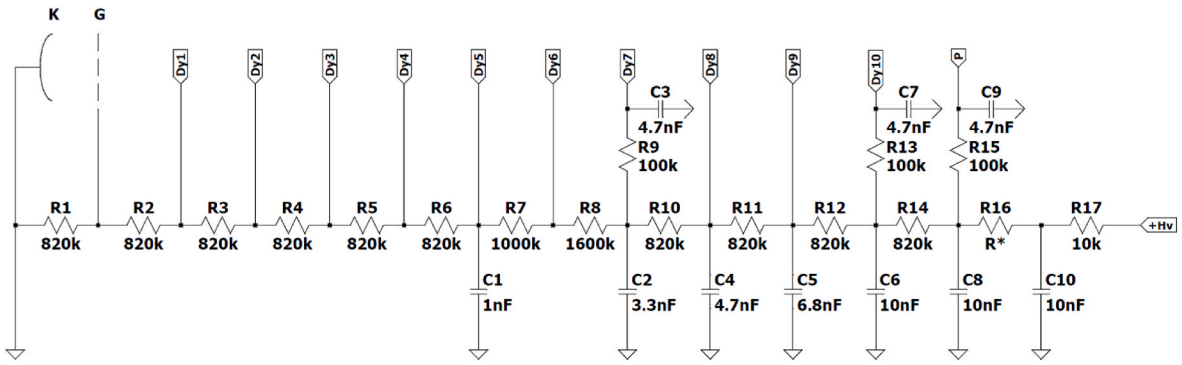


**Fig. 3.** The circuit of the optimized voltage divider for the Hamamatsu R877 PMT.

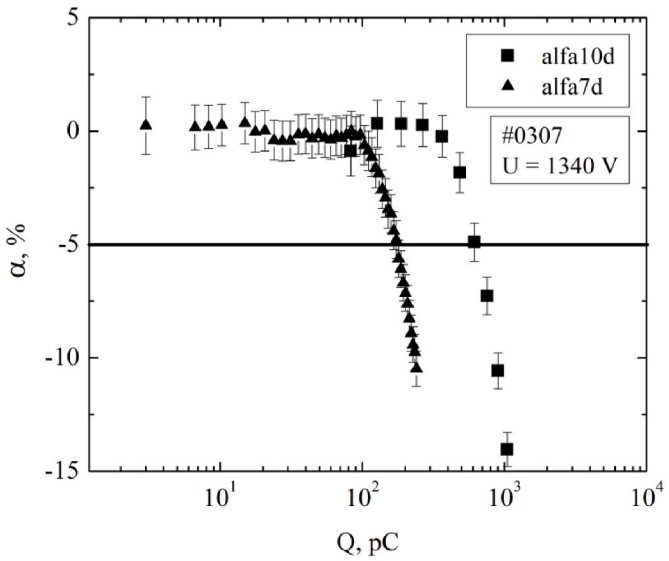


**Fig. 4.** Non-linearity coefficient α as a function of the output signal of 10th and 7th dynodes of the Hamamatsu R877 PMT.

$$P(n) = \frac{\lambda^n}{n!} \bullet e^{-\lambda}, \tag{3}$$

where λ is the average number of ejected photoelectrons. It is possible to select such intensity of illumination at which the probability of knocking out more than one photoelectron $P(n > 1)$ relative to the probability of knocking out one electron $P(1)$ does not exceed 5%:

$$\frac{P(n>1)}{P(1)} = \frac{1 - P(0) - P(1)}{P(1)} = \frac{1 - e^{-\lambda} - \lambda e^{-\lambda}}{\lambda e^{-\lambda}} < 0.05. \tag{4}$$

Inequality (4) is satisfied for $\lambda < 0.097$. However, as long as the gain of the PMT dynode system remains unknown, the average number of ejected photoelectrons cannot be calculated. Therefore, $\lambda$ can be estimated based on the efficiency of signal detection, which at $\lambda = 0.097$ is:

$$\eta = 1 - P(0) = 1 - e^{-\lambda} = 0.092. \tag{5}$$

Thus, if we use illumination at which the PMT response efficiency is approximately 10%, then the fraction of single-electron signals among the non-zero ones would be 95%.

When using the method of single-electron illumination, one of the main problems is the separation of the single-electron and the pedestal peaks. Often, a resolvable single-electron peak can be obtained at increased gain factors.

In our case, when testing the Hamamatsu R877 PMT No. 0307 with the optimized voltage divider, a resolvable single-electron peak was obtained at a supply voltage of 1600 V. The spectrum of anode signals is shown in Fig. 5. In the spectrum, a valley is observed at a value $Q_{val} = 0.2$ pC, the peak-to-valley ratio is $1.4 \pm 0.1$. The spectrum was measured in compliance with condition (5). According to this condition, 9.2% of events lie to the right of the valley: 8.8% are single-electron, 0.4% are two-electron, and the contribution of three-electron events can be neglected. To estimate ~~of~~ the single-electron peak parameters, the part of the spectrum to the right of the valley can be used. The average value and the standard deviation, calculated for the part of the spectrum located to the right of the valley, are $<Q \geq 0.43 \pm 0.01$ pC and $\sigma = 0.27$ pC. However, since the analysis excludes a small part of single-electron peak lying to the left of the valley, the obtained estimates are biased.

Since the fraction of multi-electron signals relative to single-electron ones is less than 5%, multi-electron events do not affect the position of the single-electron peak maximum. Therefore, the PMT gain can be estimated from the position of this peak [35]. For the spectrum in Fig. 5, the most probable value of the single-electron peak is $Q_{peak} = 0.35$ pC. At this supply voltage, the dynode system gain, estimated by the peak value, is $M = (2.2 \pm 0.1) \times 10^6$.

Using the obtained gain value $M = 2.2 \times 10^6$ at a supply voltage of 1600 V, we have obtained the gain factors in the voltage range 1200–1600 V in steps of 50 V. To do this, the photocathode was illuminated with flashes from a high-brightness LED ensuring the PMT response of 250 ph. e. Then the PMT supply voltage was reduced and the measurements were repeated at the same LED brightness. For a known number of knocked-out photoelectrons, the gain was determined from the average charge of the anode signals. The resulting dependence of the dynode system gain $M$ on the supply voltage $U$ is shown in Fig. 6. This

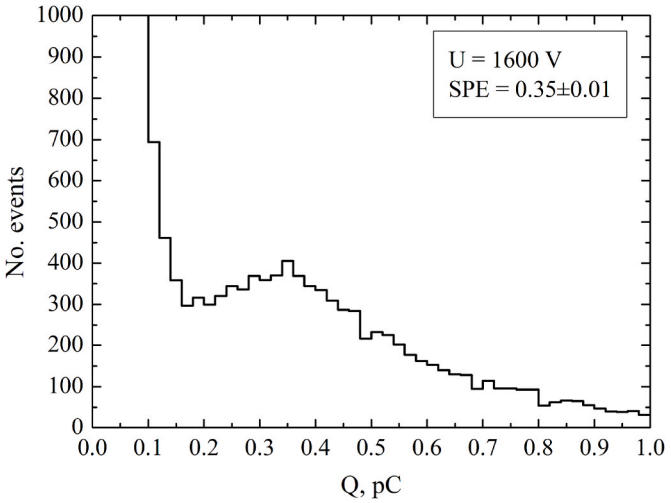


**Fig. 5.** Single-electron spectrum for Hamamatsu R877 PMT with the optimized supply voltage divider.

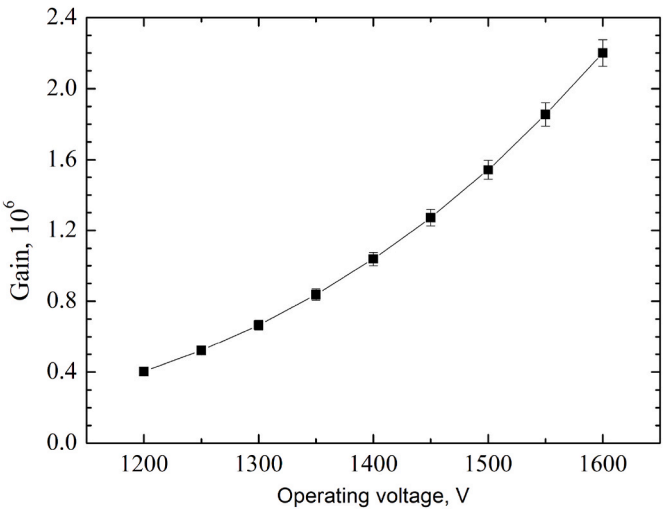


**Fig. 6.** The dependence of the dynode system gain on the supply voltage for the Hamamatsu R877 PMT.

dependence was approximated by the function:

$$M(U) = \text{const}\, U^w, \tag{6}$$

from which the exponent $w = 5.9 \pm 0.2$ was derived. In this case, the chi-squared value related to the number of degrees of freedom was $\chi^2$/d.o.f. = 0.21. The value of $w$ is consistent with the expected exponent calculated using the formula:

$$w = Nw_0, \tag{7}$$

where $N$ is the number of dynodes and $w_0$ is an empirical coefficient, that is usually in the range from 0.6 to 0.8 [36].

Using the measured gain dependence (equation (6)), we have determined that at an operating voltage of 1400 V the photomultiplier gain is $M = 10^6$. At a gain of $10^6$, we have studied the spectrometric characteristics of the Hamamatsu R877 photomultiplier in events with multi-electron illumination. For this purpose, we have measured the response spectra of Hamamatsu R877 PMT to LED illumination of various intensities. The resulting spectra had the form of a normal distribution. For each spectrum, the average PMT response $A$ and standard deviation $\sigma$ were obtained. Then the dependence of the $\sigma^2/A$ value on the PMT response $A$ was plotted (Fig. 7).

As seen, the ratio of variance to the average response does not depend on the magnitude of the response and is equal to $<\sigma^2/A> = 1.10 \pm 0.05$ ph. e. Thus, the amplitude resolution of the Hamamatsu R877 PMT can be estimated as:

$$\delta E_{\text{R877}} = \frac{\sigma}{A} = \sqrt{\frac{1.1 \text{ ph. e.}}{A}}. \tag{8}$$

Considering that with the same gain factor the resolution of the FEU-200 is $\delta E_{\text{FEU-200}} = \sqrt{1.5 \text{ ph. e.}/A}$, we find that the resolution of the Hamamatsu R877 is ~1.2 times better than that of the FEU-200. Apparently, such result is due to the fact that the Hamamatsu R877 has a box-shaped dynode system, while the FEU-200 is equipped with a louvered one.

### 2.3. Timing characteristics

For the physical analysis of events in the Cherenkov water calorimeter NEVOD, we use only amplitude information from the photomultipliers. The timing characteristics of the photomultiplier affect only the process of trigger signal formation, so there are no strict requirements for them. For generating the general trigger signal of the calorimeter, it is enough that the spread of the PMT response time (transit time spread, TTS) is less than 50–75 ns.

To estimate TTS in single-electron and multi-electron illumination modes, we have measured the distribution of PMT anode signals by arrival time. In this case, we measured the interval between the rising edge of the logical signal for LED triggering and the time when the PMT anode signal exceeded the threshold of 2 mV. The obtained distributions are presented in Fig. 8. The most probable signal arrival time for single-electron distribution is $T_{\text{peak}} = 29 \pm 1$ ns and for multi-electron distribution is $T_{\text{peak}} = 18.5 \pm 0.5$ ns. The median values of the distributions are 34 ns and 19 ns, respectively. The full width at half maximum of the distribution is taken as the TTS value. For a single-electron distribution FWHM is equal to $30 \pm 2$ ns, and for a multi-electron distribution FWHM equals to $6.5 \pm 0.5$ ns.

When measuring delay, the position of the distributions relative to the time axis depends on the length of the cables, so individual peak values do not contain any physical information. However, it can be seen that at multi-electron illumination, the most probable time of signal arrival is 10.5 ns less than that for single-electron signals. This is due to the fact that with multi-electron illumination, some photons pass through the cathode chamber and knock out photoelectrons directly from the first dynode. The measured difference between the peaks is close to the typical transit time of electrons in the cathode chamber

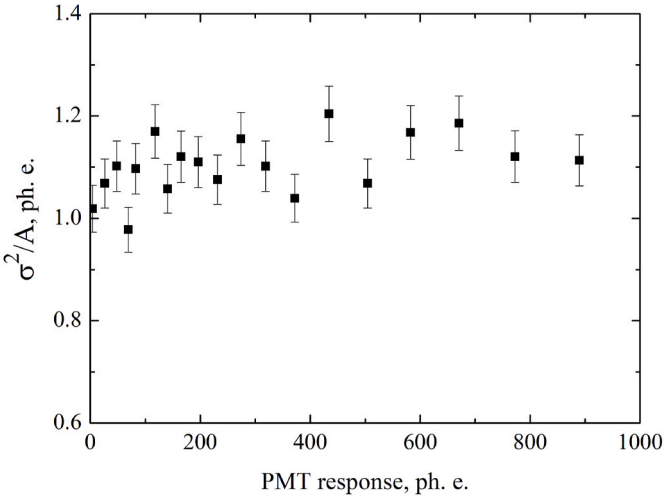


**Fig. 7.** The ratio of the variance to the average response as a function of the PMT response.

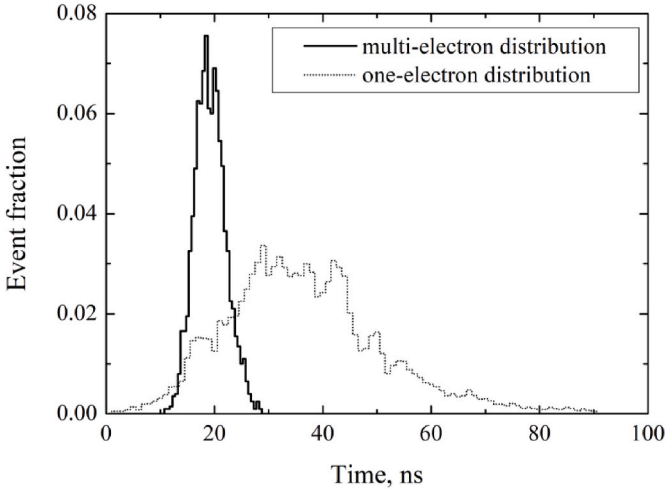


**Fig. 8.** Distribution of time delays between the LED trigger signal and the anode signal of the Hamamatsu R877 PMT.

(10–12 ns).

The TTS of multi-electron signals is significantly smaller than those of single-electron ones. It is due to the fact, that the time fluctuations of the first electrons of the avalanche in the PMT dynode system are noticeably smaller for more powerful signals. The datasheet of the Hamamatsu R877 PMT shows a TTS value of 18.5 ns for single-electron signals [32], which is ~10 ns less than the value we obtained. It is worth noting that we did not use an additional amplifier during measurements. In this case, the TTS value of single-electron signals at low thresholds may be overestimated. Therefore, the TTS value we obtained for single-electron signals should be considered as an upper limit. Since a time accuracy of 50–75 ns is sufficient to generate a trigger signal in the Cherenkov water detector, such TTS value is quite acceptable for the QSM-6M.

### 2.4. Noise characteristics

Cherenkov radiation in water is quite weak: about 200 photons are generated per centimeter of the track of a relativistic charged particle. PMTs in optical modules operate at thresholds of fractions and units of a photoelectron, so the noise counting rate is an important characteristics. The dependence of the noise signals counting rate of the PMT No. 0307 on the threshold value is shown in Fig. 9. This dependence was measured at a dynode system gain $M = 10^6$. As seen from the figure, at a threshold greater than 2.0–3.0 ph.e. the slope of the dependence changes, and the noise counting rate decreases slower. Most likely that at a threshold greater than 2.0 ph.e., almost all single-electron noise signals are cut off, and the photomultiplier detects Cherenkov light produced by background beta-decay electrons in the photocathode glass.

## 3. Electronics features

Each garland (cluster) of the Cherenkov water calorimeter NEVOD consists of 3 or 4 quasi-spherical modules and a block of electronics of the cluster (BEC). Quasi-spherical modules detect Cherenkov radiation and transmit analog PMT signals to the BEC for digitizing.

When developing the QSM-6M, we required that the design, supply voltage, control signals and output signals should be as close to the QSM-6 as possible. Such unification will make the upgrade of the Cherenkov water calorimeter as simple as possible, since one module in the detector can be replaced by another without additional operations.

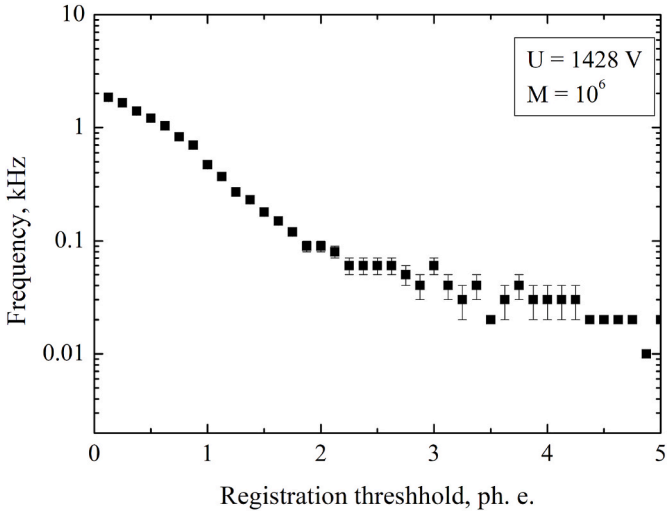


**Fig. 9.** Typical dependence of the dark noise counting rate of the Hamamatsu R877 PMT on the detection threshold.

### 3.1. Intra-modular electronics of the QSM-6M

The QSM-6M intra-modular electronics is developed based on the QSM-6 intra-modular electronics [24,37] and consists of six PKh-514 M boards, a PNN-382 power supply unit and a six-channel LED monitoring system (Fig. 10).

The circuit of the PKh-514 M board, designed to work together with the Hamamatsu R877 PMT, is close to those for the PKh-514P board that works with the FEU-200 photomultiplier. The PKh-514 M board includes the optimized supply voltage divider and two charge-sensitive amplifiers (CSAs) shaping signals from the 10th and 7th dynodes. For installation on the Hamamatsu R877 PMT, a 14-pin socket E678-14W is soldered onto the PKh-514 M.

The CSAs convert short signals from the PMT dynodes into long signals of a special form, adapted for processing by analog-to-digital converters (ADCs). The amplitude of the signal at the CSA output is proportional to the charge at the dynode. The conversion coefficients of the CSAs of the 10th and 7th dynodes are 25 mV/pC and 28.5 mV/pC, respectively.

The timing parameters of the shaped signals do not depend on the amplitude and have the following values: rising edge 50 ns, trailing edge ~2 μs. Signals from the CSA have a flat top, on which a 25 ns sample-hold ADC stores the value of the signal amplitude.

To measure the characteristics of the spectrometric route PMT→CSA→ADC, the QSM-6M intra-modular electronics provides a monitoring system based on a six-channel LS6CH controller that manages operation of six LD_DR illumination drivers with KingBright L-7113NBC LEDs. Each driver illuminates the photocathode of one PMT with short (FWHM ~7 ns) LED flashes. The controller is managed via the $I^2C$ bus.

Power supply for the PMT and all boards of intra-modular electronics is provided by the PNN-382 unit, which converts the +12 V input voltage into ±12 V and high voltage. To obtain the high voltage, a DC/DC converter TRACO POWER MHV12-2.0k1000P is used. Adjustment of the required voltage value is carried out within the range of 1000–1800 V using a variable resistor; this voltage is supplied to six PKh-514 M boards. The individual supply voltage of each PMT is set using a ballast resistor in the divider circuit of the PKh-514 M board (resistor $R_{15}$ in Fig. 3).

The total power dissipation of the intra-modular electronics does not exceed 6.5 W. The duralumin body of the quasi-spherical module acts as a radiator and transfers generated heat into the water. The annual average water temperature in the tank is 23.6 °C, and the standard deviation over the year is 0.7 °C. The small annual temperature variation ensures stable operation of the intra-modular electronics.

### 3.2. Photo-electronics unit of the QSM-6M

To protect the photomultiplier from hydrostatic pressure, a transparent protective illuminator made of organic glass is used. When developing the QSM-6M, we used the same body as for the QSM-6. However, the outer diameter of the Hamamatsu R877 PMT bulb is smaller than that of the FEU-200 PMT. So we have developed a new protective illuminator for the PMT Hamamatsu R877 (Fig. 11, left) having the same mounting diameter as the illuminator for the FEU-200. The thickness of the transparent window of the illuminator is 15 mm. A plastic inset ring is used to install the photomultiplier into the protective illuminator. To ensure the optical contact, the space between the illuminator and the entrance window of the photomultiplier is filled with transparent Penta-312 silicone gel. The final fixation of the photomultiplier is performed using a light-insulating clamping disk, a sealing ring, a stud-bolt and three M5 screws. This design prevents the through passage of Cherenkov photons inside the QSM-6M. To ensure monitoring, the illuminator has a light guide channel into which the LED of the LD_DR illumination driver is installed.

The Hamamatsu R877 photomultiplier with the PKh-514 M board,

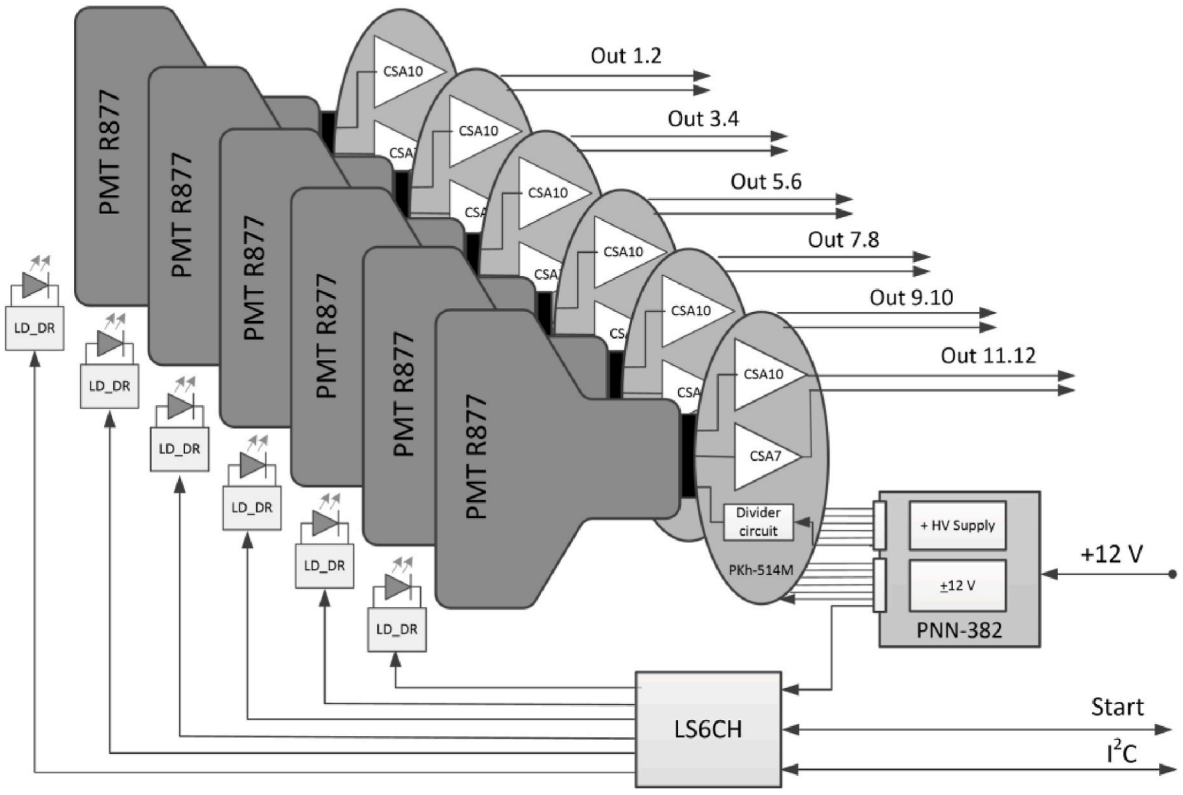


**Fig. 10.** Functional diagram of the QSM-6M intra-modular electronics.

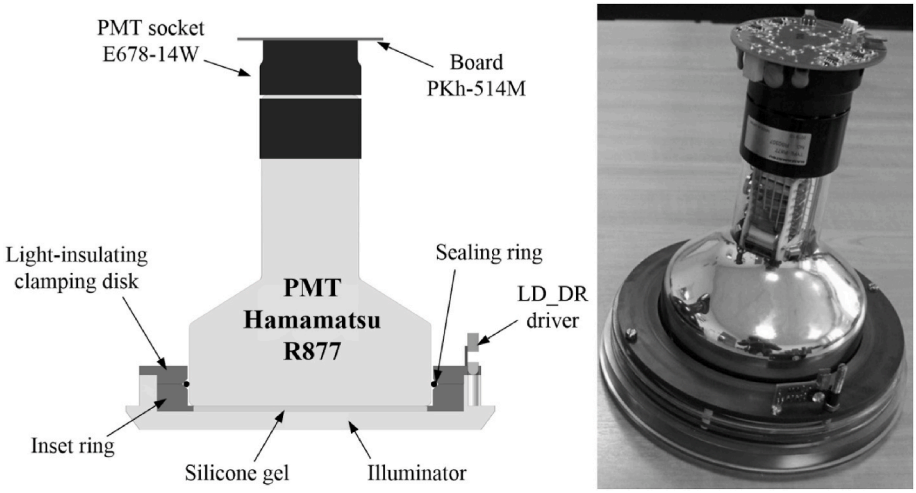


**Fig. 11.** Diagram (left) and photograph (right) of the photo-electronics unit.

the LD_DR driver and the protective window form a photo-electronics unit (Fig. 11, right).

Quasi-spherical modules QSM-6 and QSM-6M differ from each other only in photo-electronics units. Therefore, upgrade of quasi-spherical modules can be performed by replacing six photo-electronics units based on the FEU-200 with six new photo-electronics units with the Hamamatsu R877. A photograph of the quasi-spherical module QSM-6M is shown in Fig. 12.

### 3.3. Block of electronics of the cluster

In the Cherenkov water calorimeter, quasi-spherical modules of one garland (3 or 4 modules) are combined into clusters using a block of electronics of the cluster (BEC).

The BEC electronics is located in a sealed stainless steel housing installed under the tank cover, above the water level. All signals from the intra-modular electronics of each QSM are fed to the BEC via two deep-water cables. Cables are inserted into the QSM using cable glands (protection class IP68), and are connected to the BEC connectors using sealed (IP67) HUMMEL signal connectors.

Each BEC processes analog signals from the modules, controls measurements and monitoring of spectrometric channels, as well as ensures data exchange with the triggering system and the central computer of the Cherenkov water calorimeter. The BEC contains four modules of amplitude analysis MAA-01P, a processor board WAFER C400E2VN-RS, an interface module for a temperature sensor and a power module.

**Fig. 12.** Quasi-spherical module QSM-6M.

Modules of amplitude analysis MAA-01P provide parallel digitization of analog signals from two dynodes of each of six photomultipliers using 12-bit 2-channel Texas Instruments ADS7862YB ADCs.

To trigger the conversion circuit and to generate logical signals, the MAA-01P boards contain discriminators with a software-controlled threshold. The threshold setting accuracy is 0.1 mV/bit. The MAA-01P digital circuit is based on a field-programmable gate array (FPGA) Xilinx XC2S50-6PQ208C, which provides data exchange with the BEC processor board, digital processing of signals from the QSM, interaction between all components of the board and ensures blocking of spectrometric channels using software-controlled switches. The important functions of the FPGA are the measurement of PMT noise using 16-bit counters and the generation of trigger signals of three types for each QSM: "a" (any), logical "OR" of six signals from the 10th dynodes of the PMTs; "b" (bottom), signal from the PMT directed downwards (PMT-5); "c" (coincidence), coincidence of signals from any two photomultipliers, except those in opposite directions, within a time gate of 150 ns.

The MAA-01P boards have two main operating modes: monitoring and exposition. The monitoring mode is designed to check whether the detector measuring channels operates correctly. The exposition mode ensures detection of physical events using Cherenkov radiation in the working volume of the calorimeter.

Due to unification, the QSM-6M quasi-spherical module can be connected to any of the existing BECs of the Cherenkov water calorimeter.

## 4. Study of QSM-6M characteristics in water

To study the QSM-6M response to real physical events, the module was installed in the spatial lattice of the Cherenkov water calorimeter.

### 4.1. Test conditions

Cherenkov water calorimeter (Fig. 13) has a size of $9 \times 9 \times 26$ m$^3$. The spatial lattice of the calorimeter consists of 25 garlands, each of which is a cluster. Sixteen out of 25 clusters consist of 4 QSMs and form four vertical planes of 16 QSMs in each. The remaining 9 clusters consist of 3 QSMs and form three vertical planes of 9 modules in each. The distance between the modules in a garland and between the centers of the garlands in a plane is 2 m. The distance between the planes of the same type is 2.5 m. Photomultiplier tubes in quasi-spherical modules are numbered as follows: the normal to PMT-1 is directed along the Y axis, the normal to PMT-3 is directed in the opposite direction; the normal to PMT-2 is directed along the X axis, the normal to PMT-4 is opposite to the PMT-2 normal; the normal to PMT-5 is directed downwards against the Z axis, the normal to PMT-6 is directed upwards along the Z axis. The test module QSM-6M was installed in one of the clusters of four QSMs at a depth of 3 m from the water surface (Fig. 13).

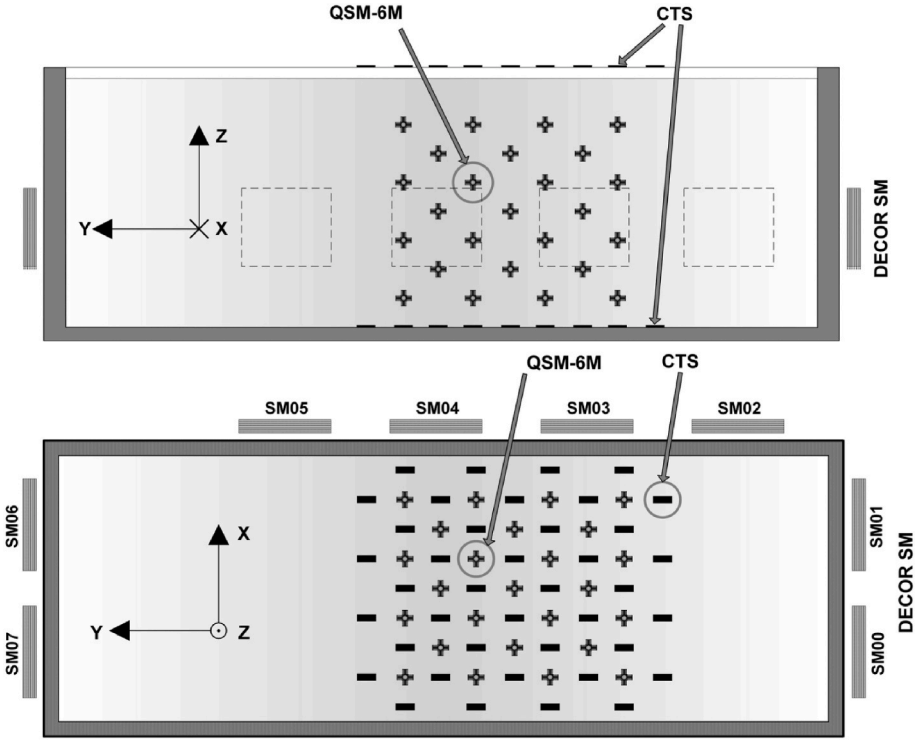


**Fig. 13.** Cherenkov water calorimeter NEVOD, system of calibration telescopes and muon-tracking detector DECOR (top: side view; bottom: top view).

On the bottom and on the top cover of the Cherenkov water calorimeter, 80 scintillation counters of the calibration telescope system are installed [38]. The scintillator size is 40 × 20 × 2 $cm^3$. Any pair of counters from the upper and lower planes forms a muon telescope. In total, there are 1600 such telescopes. The axes of vertical telescopes are located in the middle between the garlands of quasi-spherical modules.

Around the Cherenkov water calorimeter, eight supermodules (SMs) of the muon-tracking detector DECOR are located [39]. The DECOR detector has a total area of 70 $m^2$ and makes it possible to reconstruct muon tracks with a high accuracy. Supermodules of the DECOR are located in the side galleries of the first floor of the experimental complex building: two pairs of SMs are located along the short sides of the water tank, and four SMs are installed along the long side (Fig. 13, bottom).

The simplest characteristics of the optical module operating in water is the dependence of its counting rate on the detection threshold. Fig. 14 shows such dependences for all PMTs of the QSM-6M. In water, the counting rate of each photomultiplier is the sum of the counting rates of dark noise and Cherenkov radiation flashes. For most events in the water tank, direct Cherenkov light is directed from the upper to the lower hemisphere. Only in the case, when particles arrive at zenith angles greater than 48°, some part of the Cherenkov radiation photons move from the lower to the upper hemisphere. PMT-5 is oriented to the lower hemisphere and the nature of its dependence differs from other photomultipliers of the module.

Fig. 15 shows the dependences of the counting rate of the QSM-6M trigger signals on the detection threshold. Trigger signals “a” and “b” are largely dependent on the PMT noise, since trigger “a” combines the hits of all six PMTs by “OR”, and signal “b” coincides with the earlier mentioned dependence of PMT-5. Trigger “c” is weakly dependent on the PMT noise, since it is generated when the signals of two PMTs coincide. Therefore, the counting rate of trigger “c” can be considered as the counting rate of Cherenkov radiation flashes.

As a rule, detection of events in a Cherenkov water calorimeter is carried out at a threshold of 2.0 ph. e. As seen from Fig. 15, the counting rate of Cherenkov radiation flashes at this threshold is $\sim 3 \times 10^3$ $s^{-1}$.

In the period from 2021 to 04-08 to 2022-10-05 (more than 18 calendar months), the QSM-6M module was operated as a part of the detecting system of the Cherenkov water calorimeter. The total operating time was 11228 h of “live” time. The long duration of the QSM-6M operation in water provided opportunity to study in detail its characteristics when measuring events of various classes.

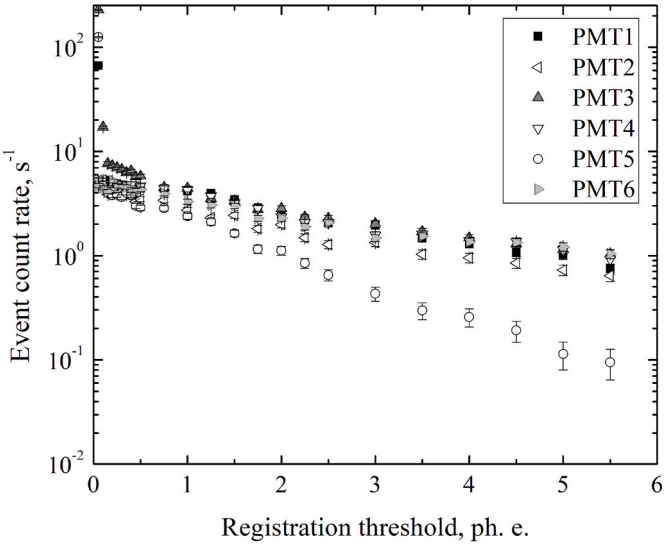


**Fig. 14.** Dependences of the counting rate of the QSM-6M photomultipliers in water on the detection threshold.

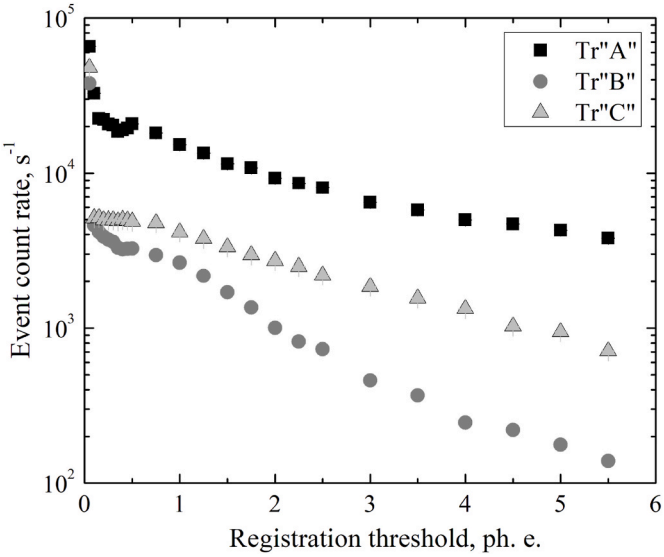


**Fig. 15.** Dependences of the counting rate of QSM-6M trigger signals in water on the detection threshold.

### 4.2. *Response of QSM-6M to single muons*

The calibration telescope system makes it possible to select single muons which are necessary for calibrating the photomultipliers of the Cherenkov water calorimeter. Around each garland there are four vertical telescopes. They allow to calibrate five of six photomultiplier tubes of the QSM. The average energy of the muons used in this case is 4 GeV. Fig. 16 shows an example of an event in which the telescope located near the QSM-6M was triggered. The crosses in the figure show triggered QSMs, the circles show triggered photomultipliers.

The response spectra of the QSM-6M photomultipliers to the telescope events are shown in Fig. 17. The calibration conditions for all QSM photomultipliers are slightly different, since the distance from the center of the garland to the axes of the telescopes is 1.25 or 1.0 m. Taking into account the dimensions of the module, we find that the distance from the centers of PMT-1 and PMT-3 to the axes of the telescopes is 0.97 m, and those for PMT-2 and PMT-4 is 0.72 m. PMT-6 can be calibrated by four

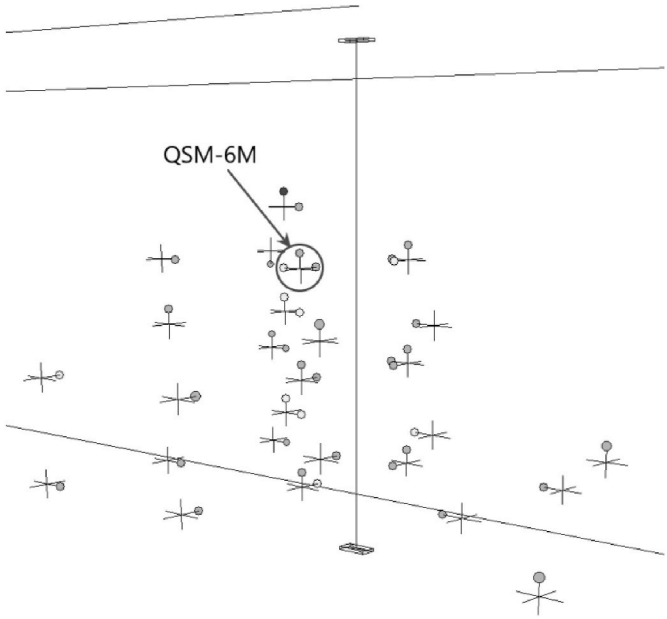


**Fig. 16.** Example of a telescope event.

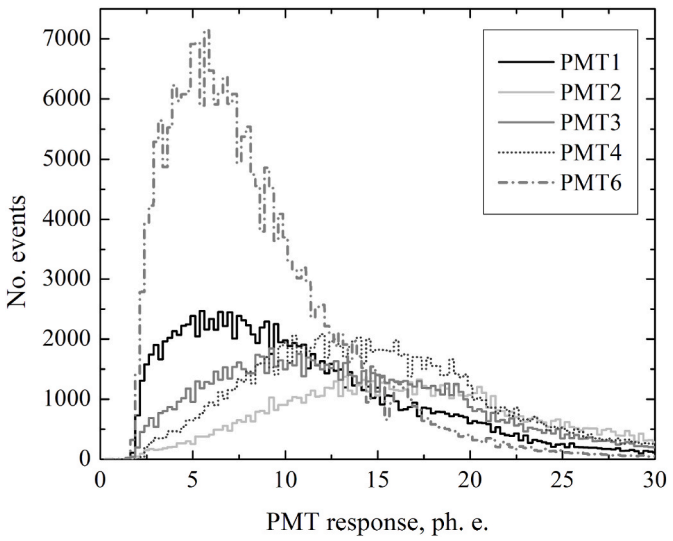


**Fig. 17.** Examples of spectra of PMT responses to telescope events.

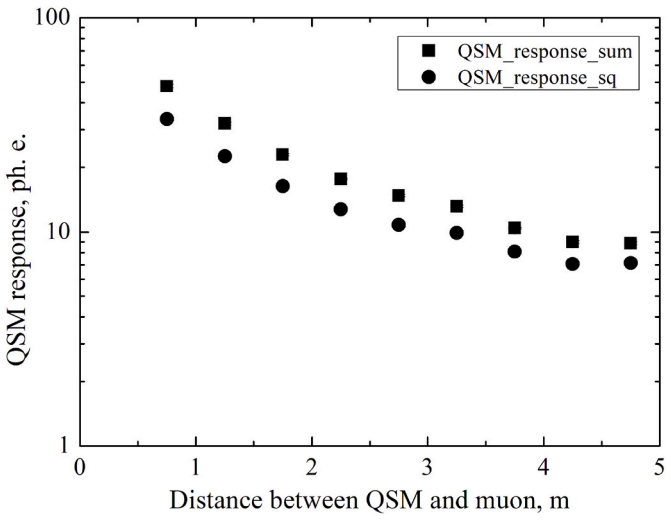


**Fig. 19.** Dependence of the average QSM-6M response on the distance to the near-horizontal muon.

telescopes at once. However, Cherenkov radiation from telescopes located at a distance of 1 m is obscured by structural elements and cable communications of the garland. Therefore, to calibrate PMT-6, we use telescopes located at a distance of 1.25 m from the center of the PMT. Also in calibration, we take into account that the angle of incidence of direct Cherenkov radiation on the photocathodes of the QSM side photomultipliers is 49°, and for the upper PMT-6 this angle is 41°.

The muon-tracking detector DECOR makes it possible to select events with single near-horizontal muons. For the analysis, we selected events in which only two DECOR supermodules, located in different short galleries, were triggered, and the tracks reconstructed based on signals of individual SMs are consistent within a cone with an opening angle of 5°. We assume that in such events, a single muon passes through both SMs, and, accordingly, the straight line, connecting the centers of coordinates of the tracks in the SMs, is taken as the muon track. The average energy of such muons is about 100 GeV. In this case, the position of the track in the water tank is known with an accuracy of several centimeters. Fig. 18 shows an example of a detected near-horizontal muon, which track was reconstructed by the data of SM01 and SM06 of the DECOR detector.

The coordinates of a single muon track, measured by the DECOR, make it possible to calculate the distance from the track to the center of a quasi-spherical module or PMT, as well as to determine the arrival direction of direct Cherenkov photons using the DECOR data.

Fig. 19 shows the dependences of the average QSM-6M responses on the distance to the muon track. The average QSM-6M response was determined in two ways: as a simple sum of the PMT responses and as the root of the sum of squares of the PMT responses.

It is worth noting that the QSM-6M response calculated using the first option is always greater than or equal to the response calculated using the second option. Since the average cosine between the normal of the PMT photocathode and the arrival direction of the Cherenkov radiation is 0.5, the sum of the amplitudes on average should be 1.5 times greater than the root of the sum of the squares of the amplitudes. For the dependences in Fig. 19, this ratio is 1.42 ± 0.01 in the range of distances from 0 to 2 m, which is close to the expected value.

Single near-horizontal muons allow calibration of the downward oriented PMT-5. Fig. 20 shows the spectrum of PMT-5 responses to single near-horizontal muons. For calibration, we selected muons that passed at a distance from 0.8 to 1.1 m to PMT-5. In this case, the average distance is 0.97 m, and the cosines of the incidence angles of Cherenkov radiation to the PMT-5 normal are in the range from 0.50 to 0.55 with an average value of 0.528.

Table 1 shows the average responses of the QSM-6M photomultiplier to single muons. The response of PMT-5 was determined from near-horizontal muons recorded by the DECOR, and the responses of the remaining PMTs were determined from vertical muons recorded by the CTS. Based on the average PMT response, on the distance from the PMT to the track and on the cosine of the incidence angle of the Cherenkov radiation, the relative sensitivity coefficients of the photomultipliers were estimated:

$$S = \frac{A \bullet R}{\cos\alpha \bullet A_0}, \tag{9}$$

where $A_0 = 17.8$ ph.e. is an expected PMT response at a distance $R = 1$ and a cosine of incidence angle $\cos\alpha = 1$. When calculating the relative sensitivity for PMT-5, it was taken into account that due to the significant difference in average muon energies, the response to near-

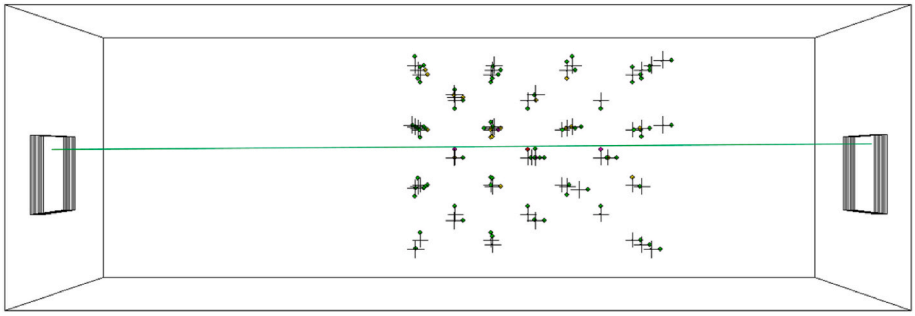

**Fig. 18.** Example of the detection of near-horizontal muon.

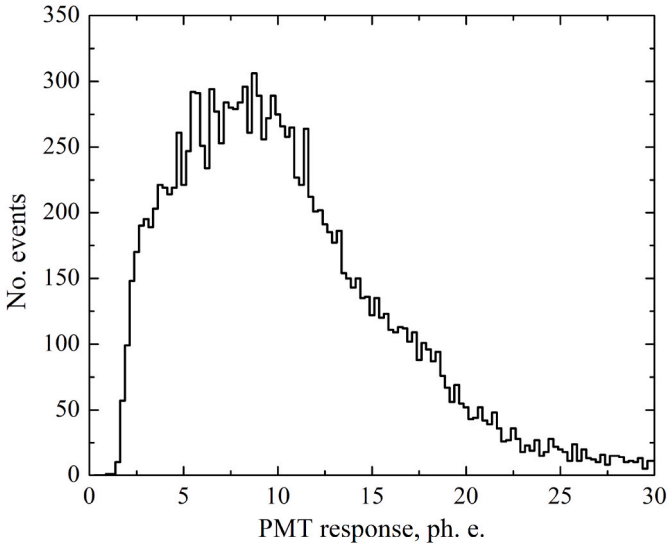


**Fig. 20.** The spectrum of the PMT-5 responses to the near-horizontal muons.

**Table 1**
Average responses of the QSM-6M PMTs to single muons.

| No. PMT | R, m | Cosine of incidence angle $\alpha$ | Average PMT response $A$, ph. e. | Relative sensitivity $S$ |
|---|---|---|---|---|
| 1 | 0.97 | 0.662 | 11.4 | 0.94 |
| 2 | 0.72 | 0.662 | 19.2 | 1.17 |
| 3 | 0.97 | 0.662 | 14.5 | 1.19 |
| 4 | 0.72 | 0.662 | 16.2 | 0.99 |
| 5 | 0.97 | 0.528 | 10.9 | 1.02 |
| 6 | 1.25 | 0.750 | 7.5 | 0.70 |

horizontal muons is about 10% higher than the response to vertical ones.

Using data on the PMT relative sensitivity, we have obtained the dependence of the response of the photo-electronics unit based on the Hamamatsu R877 PMT on the cosine of the incidence angle of the Cherenkov radiation at the photocathode (Fig. 21). The dependence was measured using near-horizontal muons that passed at an average distance $<R \geq 1$ m from the center of the QSM-6M.

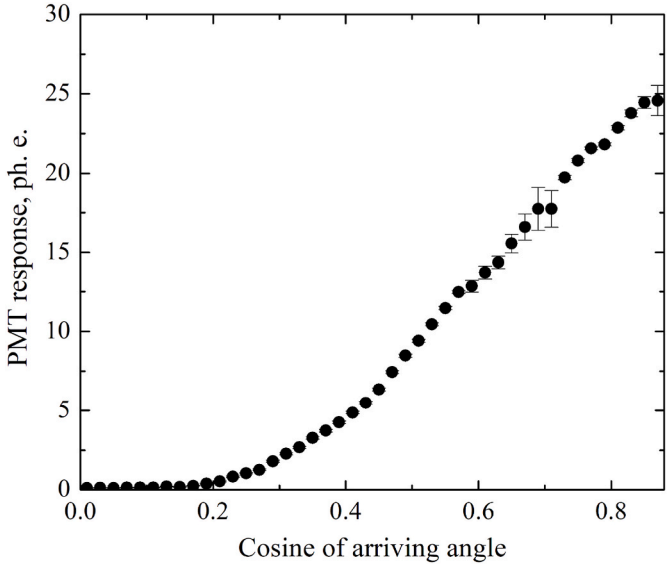


**Fig. 21.** Dependence of the response of the photo-electronics unit based on Hamamatsu R877 PMT on the cosine of the Cherenkov radiation incidence angle.

Based on the responses of the QSM-6M photomultipliers, it is possible to reconstruct the arrival direction of the Cherenkov radiation. In this case, the most accurate reconstruction is achieved when using the difference in responses of oppositely directed photomultipliers:

$$n_{x,y,z} = \frac{A_{2,1,6} - A_{4,3,5}}{\sqrt{(A_2 - A_4)^2 + (A_1 - A_3)^2 + (A_6 - A_5)^2}}, \quad (10)$$

where $A_i$ is response of the $i$-th PMT, $n_x$, $n_y$, $n_z$ are components of the reconstructed normal of the Cherenkov radiation front.

The arrival directions of the Cherenkov radiation reconstructed from the QSM-6M response were compared with the expected directions obtained based on the trajectory of single muons recorded by the DECOR. Fig. 22 shows the distribution of events by the cosine of the angle between the expected and reconstructed arrival direction of the Cherenkov radiation.

As seen from Fig. 22, a single QSM allows reconstructing of the Cherenkov radiation direction with a good accuracy. The average cosine of the angle is $0.85 \pm 0.02$, which corresponds to about 30°.

### 4.3. Sphericity of the QSM-6M response

When proposing the concept of a quasi-spherical module, it was assumed that the PMT response is proportional to the cosine of the angle of incidence of Cherenkov radiation at the photocathode. Further in the paper, we will call such PMTs the model ones. In this case, the QSM-6 response, calculated as the root of the sum of squares of the responses of model PMTs, does not depend on the arrival direction of the Cherenkov radiation. But if we use the simple sum of PMT responses as the QSM-6 response, then it depends on the arrival direction of the Cherenkov radiation. The expected response of QSM-6, consisting of model PMTs, is shown in Fig. 23. The module has a minimal response in the case when the Cherenkov radiation arrives perpendicularly to the photocathode of one of the PMTs, and has a maximal response if the Cherenkov radiation arrives at equal angles to three PMTs at once ($\cos\alpha = \sqrt{3}/3$). The maximal response is $\sqrt{3}$ times greater than the minimal one. The average response is 1.5 times greater than the minimal one.

To estimate the sphericity of the module the following parameter is used:

$$S = \left(1 - \frac{\sigma}{< A >}\right) 100\%, \quad (11)$$

where $<A>$ is an average response of the optical module, $\sigma$ is the

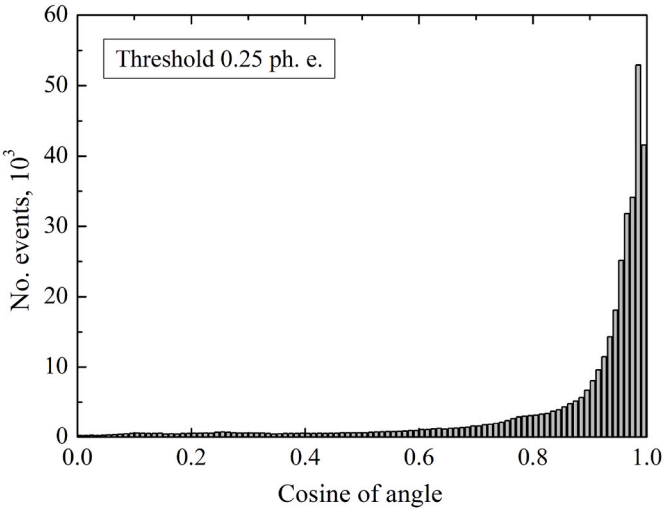


**Fig. 22.** Distribution of events by the cosine between the expected and reconstructed directions of the Cherenkov radiation.

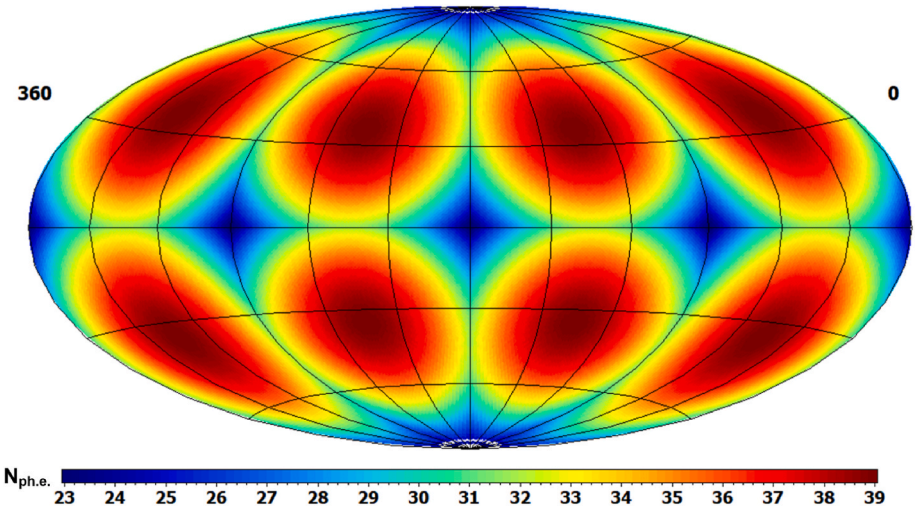


**Fig. 23.** Expected response of QSM-6, calculated as a simple sum of PMT responses (in photoelectrons), in the case where the PMT response is proportional to the cosine of the Cherenkov radiation incidence angle.

response r.m.s. deviation. For QSM-6, consisting of model PMTs, the response sphericity calculated as the simple sum of the PMT responses is 89.8%, and the response sphericity calculated as the root of the sum of squares of the PMT responses is 100%.

As seen from Fig. 21, the response of a real photo-electronics unit based on Hamamatsu R877 PMT differs from the model PMT response, which should be strictly proportional to the cosine of the angle of incidence of the wave front. This difference is due to optical effects occurring at the boundaries of the media: water – organic glass of the illuminator – silicone gel – photocathode glass – vacuum inside the bulb. Based on the experimental dependence of the response of the photo-electronics unit on the cosine of the incidence angle of the Cherenkov radiation, the similar dependences were calculated for the response of the QSM-6M. Fig. 24 shows the dependence of the QSM-6M response calculated as a simple sum of the responses of the photomultipliers. The dependence of the QSM-6M response calculated as the root of the sum of squared responses of the photomultipliers is shown in Fig. 25.

As seen from Fig. 24, qualitatively the response of QSM-6M, calculated as a simple sum of responses of photo-electronics units, is close to the model response of the QSM-6 (see Fig. 23). The minimal response is observed when the photomultipliers are illuminated perpendicularly. An increased response is observed when two or three photomultipliers are simultaneously illuminated. The response sphericity is 92.9%, which is even higher than the response sphericity of the model QSM-6.

When calculating the QSM-6M response as the root of the sum of squared responses of the Hamamatsu R877 PMT, the maximum response is observed when the photocathodes are frontally illuminated. The minimum response is observed if the Cherenkov radiation illuminates three PMTs at once (Fig. 25). In this case, the response sphericity is 91.4%. Thus, the sphericity of the QSM-6M response weakly depends on the method of its calculation.

### 4.4. *Response of the QSM-6M in multi-particle events*

To expand the dynamic range of recorded signals, the QSM-6M uses dual-dynode signal readout from the 10th and 7th dynodes of the Hamamatsu R877 photomultiplier. The crosslinking coefficient is individual for each photomultiplier and is determined by events with high illumination, when a large number of charged particles are recorded in the detector volume. Fig. 26 shows the correlation of the responses of the 10th and 7th dynodes of the PMT-2 in the QSM-6M in water. Blocks of electronics of clusters use 12-bit ADCs. Therefore, the maximal response that can be obtained is 4095 LSB units of the ADC. The crosslinking coefficient is determined as a mean ratio between the responses of the 10th and the 7th dynodes in events in which the response from the 10th dynode is in the range from 500 to 3500 LSB units of the ADC. For the

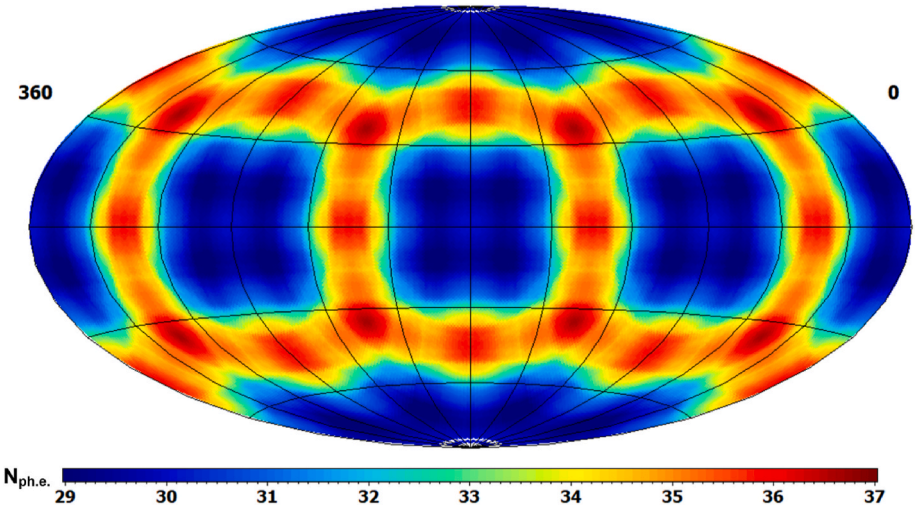


**Fig. 24.** –Response of QSM-6M, calculated as a simple sum of responses (in photoelectrons) of photo-electronics units based on Hamamatsu R877 PMT.

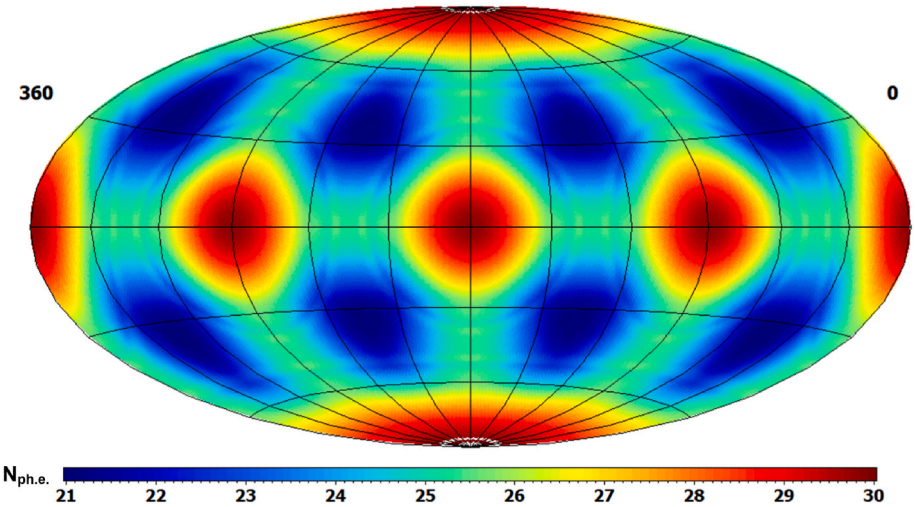


**Fig. 25.** Response of QSM-6M, calculated as a root of the sum of squared responses (in photoelectrons) of photo-electronics units based on Hamamatsu R877 PMT.

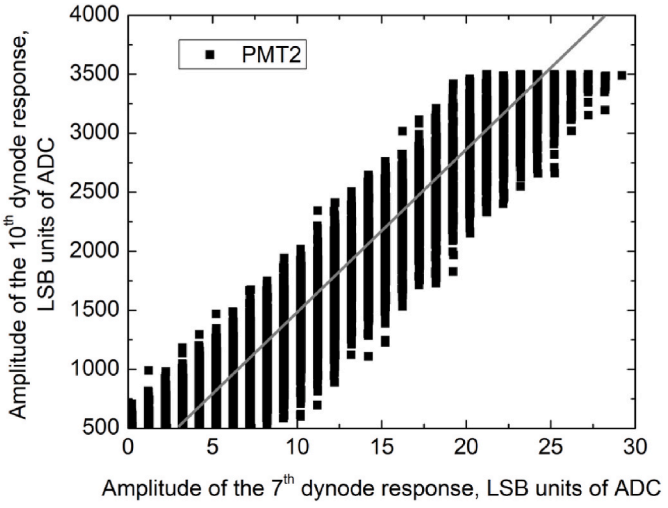


**Fig. 26.** Correlation of responses of the 10th and 7th dynodes of the PMT-2 of the QSM-6M in events with high illumination in the Cherenkov water calorimeter.

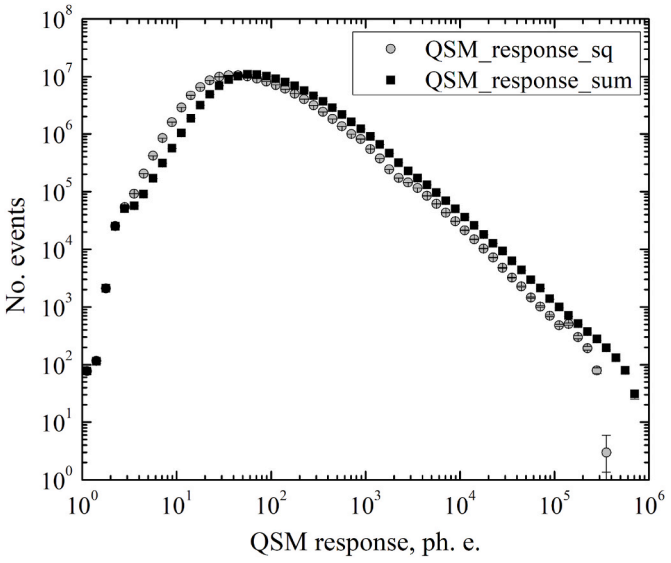


**Fig. 27.** Spectrum of QSM-6M responses in multi-particle events.

PMT-2 of the QSM-6M, the crosslinking coefficient is 138.9 ± 0.4, and the correlation coefficient is 0.96 ± 0.02 (line in Fig. 26). The cross-linking coefficients of the remaining QSM-6M photomultipliers are in the range from 130 to 158.

Using the obtained crosslink coefficients for the ranges of 10th and 7th dynodes, we have analyzed the QSM-6M response in multi-particle events. To select multi-particle events, the Cherenkov water calorimeter has a special trigger "60c", which is generated in case of simultaneous hit of at least 60 QSMs with trigger "c". As a rule, such events are associated with the detection of extensive air showers, muon bundles or cascade showers initiated by single muons in the detector volume.

Fig. 27 shows the spectrum of QSM-6M responses in multiparticle events. The QSM-6M response was determined in two ways: as a simple sum of the PMT responses and as the root of the sum of squares of the PMT responses. When approximating the spectrum in the response range from ~$10^3$ to $10^5$ ph. e. with a power-law dependence

$$\frac{dN}{dA} = CA^{\beta}, \tag{12}$$

for the spectrum of QSM-6M responses, defined as the sum of the PMT responses, we have obtained the slope index $\beta = -2.47 \pm 0.01$. For the QSM-6M response, defined as the root of the sum of squares of the PMT response, the slope index is $\beta = -2.51 \pm 0.02$.

Since the main recorded multi-particle events are extensive air showers, the spectrum of QSM-6M responses should be close to the spectrum of the EAS sizes. The review [40] presents the results of measuring EAS size spectra obtained in various experiments. According to these results, the exponent of the EAS size spectrum is in the range from $\beta = -2.3$ to $\beta = -2.8$. In the EAS size spectrum measured at the NEVOD-EAS array the slope index is $\beta = -2.49 \pm 0.03$ [41].

Since the slopes of the QSM-6M response spectra are close to the results of other experiments, this demonstrates that the QSM-6M is capable of recording signals of up to about $10^5$ ph. e. This dynamic range is a record one for optical modules of Cherenkov detectors.

### 4.5. Cascade showers in water

A dense spatial lattice of quasi-spherical modules makes it possible to reconstruct cascade curves of showers generated by muons in the volume of the Cherenkov water calorimeter [42]. The reconstruction technique is based on the amplitude analysis of the response of photomultipliers that record direct Cherenkov radiation from the cascade axis

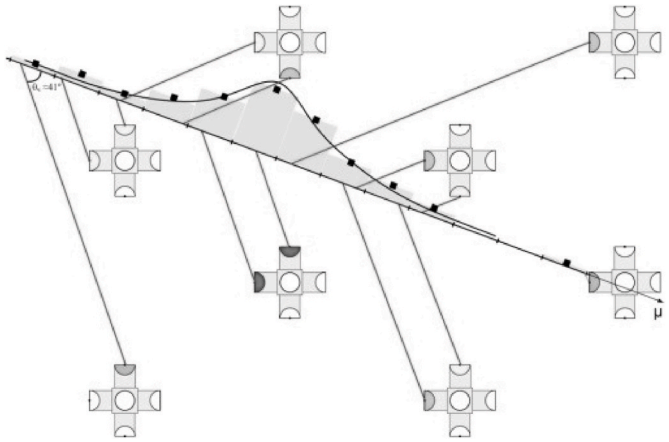

**Fig. 28.** –Diagram of measuring a cascade-shower curve in the Cherenkov water calorimeter.

(Fig. 28). It is assumed that: electrons generated in the shower move along the cascade axis; cascade axis coincides with the muon track; all Cherenkov photons are emitted at the same angle to the axis $\theta_C = 41°$. The coordinates of the muon track are measured using the DECOR detector. The axis of the cascade is divided into segments of one radiation unit in water (36.1 g/cm$^2$). Each such segment can be viewed by several photomultipliers, which makes it possible to determine the number of charged particles in this segment.

Fig. 29 shows an example of a reconstructed cascade curve of a shower with energy of about 1.5 TeV. The squares represent the number of charged particles measured according to the data of the QSM-6 with the FEU-200 PMTs. The stars represent the number of charged particles determined from the data of the Hamamatsu R877 photomultipliers in the QSM-6M (2 out of 6 PMTs recorded direct Cherenkov radiation). The curve is the Greisen approximation for the cascade curve [43]:

$$N(t) = \frac{0.32}{\sqrt{y_0}} \exp((t - t_0)(1 - 1.5s)), \tag{13}$$

$$s = \frac{3(t - t_0)}{(t - t_0) + 2y_0}, \tag{14}$$

where $y_0 = \ln(E/\varepsilon)$, $E$ is a cascade energy, $\varepsilon = 73$ MeV is a critical energy of electrons in water, $s$ is a shower age, $t$ is measured in radiation units, $t_0$ is a shower generation point.

As seen from Fig. 29, there is good agreement between the numbers of charged particles determined from the data of the QSM-6 and QSM-6M.

For events with cascade showers, we have obtained a correlation between the numbers of charged particles determined from the data of the QSM-6M and QSM-6. We analyzed cascade events with energies from 5 GeV to 2 TeV. The correlation is shown in Fig. 30. The correlation coefficient is 0.87 ± 0.32. The dependence was approximated with a straight line, the slope of which was 0.95 ± 0.02. The closeness of the slope coefficient to 1.0 indicates that the calibration coefficients for QSM-6M were determined correctly.

Thus, the analysis of the QSM-6M response in events with large illumination made it possible to check the dynamic range of the module, and to calibrate its multi-particle response in the cascade-shower events.

## 5. Conclusion

The developed optical module QSM-6M, which is based on the Hamamatsu R877 photomultiplier, is capable of detecting Cherenkov radiation in water in a solid angle of 4π in the dynamic range from 1 to more than $10^5$ ph. e. Based on the response of a single QSM-6M module, it is possible to determine the arrival direction of Cherenkov radiation in water with an accuracy of ~30°. The sphericity of the module is 92.9%.

The QSM-6M modules will be used to expand the detecting system of the Cherenkov water calorimeter NEVOD. The developed methods for measuring characteristics of optical modules will be used for testing optical modules of neutrino telescopes inside the volume of Cherenkov water calorimeter NEVOD.

### CRediT authorship contribution statement

**M.B. Amelchakov:** Writing – original draft, Investigation. **A.G. Bogdanov:** Writing – original draft, Investigation. **A. Chiavassa:** Writing – review & editing. **D.M. Gromushkin:** Writing – original draft, Investigation. **A.N. Dmitryeva:** Writing – original draft, Investigation. **T.A. Karetnikova:** Writing – original draft, Investigation. **S.S. Khokhlov:** Writing – review & editing, Investigation. **V.V. Kindin:** Writing – original draft, Investigation. **R.P. Kokoulin:** Writing – original draft, Investigation. **K.G. Kompaniets:** Writing – original draft, Investigation. **A. Yu Konovalova:** Writing – original draft, Investigation. **G. Mannocchi:** Investigation. **N.A. Pasyuk:** Writing – original draft,

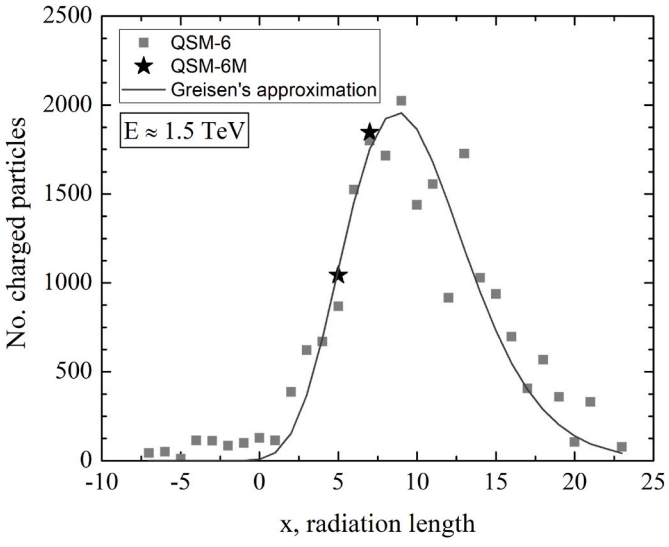


**Fig. 29.** An example of a cascade curve reconstructed according to the QSM-6 and QSM-6M data.

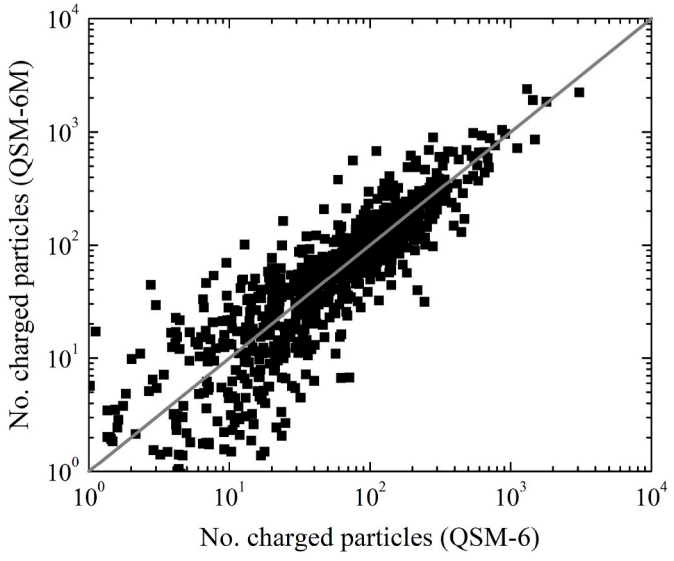


**Fig. 30.** Correlation of the numbers of charged particles obtained according to QSM-6M and QSM-6 data in events with cascade showers.

Investigation. **A.A. Petrukhin:** Writing – review & editing, Investigation. **I.A. Shulzhenko:** Writing – original draft, Investigation. **V.V. Shutenko:** Writing – original draft, Investigation. **G. Trinchero:** Investigation. **I.I. Yashin:** Writing – original draft, Investigation.

## Declaration of competing interest

The authors declare that they have no known competing financial interests or personal relationships that could have appeared to influence the work reported in this paper.

## Data availability

Data will be made available on request.

## Acknowledgments

The work was performed at the Unique Scientific Facility "Experimental Complex NEVOD" with the partial support of the Ministry of Science and Higher Education of the Russian Federation (project "Neutrino detectors for remote monitoring of nuclear power plants and astrophysical installations" No. FSWU-2022-0018). Analysis of experimental data on operation of the QSM-6M module inside the CWC NEVOD was performed using the hardware and software system for storage and analysis of large amounts of data, which is being developed with the support of the Russian Science Foundation (grant No. 22-72-10010, https://rscf.ru/project/22-72-10010/).

## References

[1] P.A. Cerenkov, Visible radiation produced by electrons moving in a medium with velocities exceeding that of light, Phys. Rev. 52 (1937) 378–379.
[2] R. Becker-Szendy, M. Bionta, C.B. Bratton, D. Casper, R. Claus, et al., IMB-3: a large water Cherenkov detector for nucleon decay and neutrino interactions, Nucl. Instrum. Methods A 324 (1993) 363–382.
[3] K.S. Hirata, T. Kajita, M. Koshiba, M. Nakahata, Y. Oyama, et al., Observation in the Kamiokande-II detector of the neutrino burst from supernova SN1987A, Phys. Rev. D 38 (1988) 448.
[4] J. Boger, R.L. Hahn, J.K. Rowley, A.L. Carter, B. Hollebone, et al., The sudbury neutrino observatory, Nucl. Instrum. Methods A. 449 (2000) 172–207.
[5] S. Fukuda, Y. Fukuda, T. Hayakawa, E. Ichihara, M. Ishitsuka, et al., The Super-Kamiokande detector, Nucl. Instrum. Methods A. 501 (2003) 418–462.
[6] DUMAND Collaboration, DUMAND II Proposal, Hawaii DUMAND Center, August 1988. HDC-2-88.
[7] A. Roberts, The birth of high-energy neutrino astronomy: a personal history of the DUMAND project, Rev. Mod. Phys. 64 (1992) 259–312.
[8] G. van Aller, S.O. Flyckt, W. Kuhlet, et al., An electro-optical pre-amplifier photomultiplier combination with Integrated power supply offering excellent single electron resolution for DUMAND, IEEE Trans. Nucl. Sci. NS- 30 (1) (1983) 469–474.
[9] V.V. Borog, S.B. Gavshin, A.A. Petrukhin, G.A. Potapov, V.V. Shestakov, Measuring module for registration of Cherenkov radiation in the water, Proc. 16th International Cosmic Rays Conference (ICRC) 10 (1979) 380. Kyoto, Japan.
[10] A.A. Petrukhin, Cherenkov water detector NEVOD and its further development, Nucl. Instrum. Methods A 952 (2020) 161585.
[11] A.A. Petrukhin, Cherenkov water detector NEVOD, Phys. Usp. 58 (2015) 486–494.
[12] V.M. Aynutdinov, V.V. Kindin, A.A. Petrukhin, V.V. Shutenko, I.I. Yashin, Cosmic ray neutrino detection on the ground level, Nucl. Phys. B 66 (1998) 235–238.
[13] S. Matsuno, J. Babson, J.G. Learned, D. O'Connor, P.K.F. Grieder, et al., Single photon light detector for deep ocean applications, Nucl. Instrum. Methods A 276 (1989) 359–366.
[14] R.I. Bagduev, V. Balkanov, I.A. Belolaptikov, L.B. Bezrukov, N.M. Budnev, et al., The optical module of the Baikal deep underwater neutrino telescope, Nucl. Instrum. Methods A 420 (1999) 138–154.
[15] A.D. Avrorin, A.V. Avrorin, V.M. Aynutdinov, R. Bannash, I.A. Belolaptikov, et al., The optical module of Baikal-GVD, Europ, Phys. J. Web Conf. 116 (2016) P01003.
[16] E. Andres, P. Askebjer, S.W. Barwick, R. Bay, L. Bergström, et al., The AMANDA neutrino telescope: principle of operation and first results, Astropart. Phys. 13 (2000) 1–20.
[17] K. Hanson, O. Tarasov, Design and production of the IceCube digital optical module, Nucl. Instrum. Methods A 567 (2006) 214–217.
[18] M. Ageron, J.A. Aguilar, I. Al Samarai, A. Albert, F. Ameli, et al., ANTARES: the first undersea neutrino telescope, Nucl. Instrum. Methods A 656 (2011) 11–38.
[19] P. Amram, M. Anghinolfi, S. Anvar, F.E. Ardellier-Desages, E. Aslanides, et al., The ANTARES optical module, Nucl. Instrum. Methods A 484 (2002) 369–383.
[20] S. Adrian-Martínez, M. Ageron, F. Aharonian, S. Aiello, A. Albert, et al., Letter of intent for KM3NeT 2.0, J. Phys. G: nucl. Part, Phys. Met. 43 (2016) 084001.
[21] S. Aiello, A. Albert, M. Alshamsi, S. Alves Garre, Z. Aly, et al., The KM3NeT multi-PMT optical module, J. Instrum. 17 (2022) P07038.
[22] S. Mechbal, N. Feigl for the IceCube Collaboration, Characterization and testing of the IceCube upgrade mDOM, Proc. 38th International Cosmic Rays Conference (ICRC) 444 (2023) 1183. Nagoya, Japan.
[23] R. Abbasi, M. Ackermann, J. Adams, N. Aggarwal, J.A. Aguilar, et al., D-Egg: a dual PMT optical module for IceCube, J. Instrum. 18 (2023) P04014.
[24] V.V. Kindin, M.B. Amelchakov, N.S. Barbashina, A.G. Bogdanov, E.A. Zadeba, et al., A Cherenkov water calorimeter based on quasi-spherical modules, Instrum. and Experim, Techniques 61 (2018) 649–657.
[25] S.S. Khokhlov, A.G. Bogdanov, V.A. Khomyakov, V.V. Kindin, R.P. Kokoulin, et al., Cascade showers in the Cherenkov light in water, Nucl. Instrum. Methods A 952 (2020) 161850.
[26] R.P. Kokoulin, N.S. Barbashina, A.G. Bogdanov, S.S. Khokhlov, V.A. Khomyakov, et al., Measuring the Cherenkov light yield from cosmic ray muon bundles in the water detector, Nucl. Instrum. Methods A 952 (2020) 161586.
[27] I.I. Yashin, M.B. Amelchakov, I.I. Astapov, N.S. Barbashina, A.G. Bogdanov, et al., Nevod – an experimental complex for multi-component investigations of cosmic rays and their interactions in the energy range 1–10^10 GeV, J. Instrum. 16 (2021) T08014.
[28] A.G. Bogdanov, R.P. Kokoulin, G. Mannocchi, A.A. Petrukhin, O. Saavedra, et al., Investigation of very high energy cosmic rays by means of inclined muon bundles, Astropart. Phys. 98 (2018) 13–20.
[29] A.A. Petrukhin, Muon puzzle in cosmic ray experiments and its possible solution, Nucl. Instrum. Methods Phys. Res. 742 (2014) 228–231.
[30] H. Dembinski, J.C. Arteaga-Velázquez, L. Cazon, R. Conceição, J. Gonzalezet al, Report on tests and measurements of hadronic interaction properties with air showers, Europ. Phys. J. Web Conf. 210 (2019) 02004.
[31] E.A. Zadeba, N.V. Ampilogov, N.S. Barbashina, A.A. Borisov, R.P. Kokoulin, et al., The detector on the basis of drift chambers for inclined muon bundle investigations, J. Instrum. 12 (2017) C07005.
[32] Datasheet of the Hamamatsu R877 photomultiplier tube, available at https://www.hamamatsu.com (accessed on April 18th, 2024).
[33] O.I. Likiy, N.V. Ampilogov, I.I. Astapov, N.S. Barbashina, N.N. Kamlev, et al., Investigating the characteristics of scintillation detectors for the NEVOD-EAS experiment, Instrum. Exp. Tech. 59 (2016) 781–788.
[34] Datasheet of the KingBright L-7113NBC light-emitting diode, available at https://www.datasheets360.com (accessed on April 18th, 2024).
[35] V.M. Aynutdinov, C.B. Bonifazi, A. Creusot, D. Dornic, B. Genolini, et al., For pierre auger collaboration, the pierre auger surface detector led flashers and their use for monitoring and calibration, Proc. 28th International Cosmic Ray Conference (ICRC), Tsukuba, Japan 2 (2003) 825.
[36] Claus Grupen and Boris Shwartz, Particle Detectors, second ed., Cambridge University Press, Cambridge, 2008.
[37] V.V. Kindin, M.B. Amelchakov, N.S. Barbashina, V.D. Burtsev, S.S. Khokhlov, et al., Cherenkov water detector NEVOD: a new stage of development, Phys. Procedia 74 (2015) 435–441.
[38] M.B. Amelchakov, A.G. Bogdanov, E.A. Zadeba, V.V. Kindin, R.P. Kokoulin, et al., The calibration telescope system of the NEVOD Cherenkov water detector, Instrum. and Experim, Techniques 61 (2018) 673–679.
[39] N.S. Barbashina, A.A. Ezubchenko, R.P. Kokoulin, K.G. Kompaniets, A. A. Konovalov, et al., A coordinate detector for studying horizontal fluxes of cosmic rays, Instrum. Exp. Tech. 43 (2000) 743–746.
[40] P.K.F. Grieder, Extensive air showers: high energy phenomena and astrophysical aspects, in: A Tutorial, Reference Manual and Data Book, Springer, Berlin, Germany, 2010.
[41] M.B. Amelchakov, N.S. Barbashina, A.G. Bogdanov, A. Chiavassa, D. M. Gromushkin, et al., The NEVOD-EAS air-shower array, Nucl. Instrum. Methods A 1026 (2022) 166184.
[42] S.S. Khokhlov, A.V. Borshevsky, D.V. Chernov, A.N. Dmitrieva, L.I. Dushkin, et al., Measurements of the energy spectrum of cascade showers initiated by muons in the Cherenkov water calorimeter NEVOD, J. Phys. Conf. 409 (2013) 012134.
[43] S. Hayakawa, Cosmic Ray Physics, Wiley, Interscience, New York, 1969.